Neuroepithelial progenitors generate and propagate non-neuronal action potentials across the spinal cord

Kalaimakan Hervé Arulkandarajah, Guillaume Osterstock, Agathe Lafont, Hervé Le Corronc, Nathalie Escalas, Silvia Corsini, Barbara Le Bras, Linda Chenane, Juliette Boeri, Antonny Czarnecki, et al.

Version of Record: https://www.sciencedirect.com/science/article/pii/S0960982221011234
Manuscript_89fe5c3a16d8bced4b468141f4021fec

Title: Neuroepithelial progenitors generate and propagate non-neuronal action potentials across the spinal cord

Authors: Kalaimakan Hervé Arulkandarajah[1#], Guillaume Osterstock[1#], Agathe Lafont[1], Hervé Le Corronc[1,2], Nathalie Escalas[3], Silvia Corsini[1], Barbara Le Bras[1], Linda Chenane[1], Juliette Boeri[1], Antonny Czarnecki[1], Christine Mouffle[1], Erika Bullier[1], Elim Hong[1], Cathy Soula[3], Pascal Legendre[1] and Jean-Marie Mangin*[1]

*These authors contributed equally.*

Author Affiliations:

[1]Sorbonne Université, INSERM, CNRS, Neurosciences Paris Seine - Institut de Biologie Paris Seine (NPS - IBPS), 75005 Paris, France

[2]Université d'Angers, 49000 Angers, France

[3]Centre de Biologie du Développement (CBD) CNRS/UPS, Centre de Biologie Intégrative (CBI), Université de Toulouse, 31000 Toulouse, France.

***Corresponding author and Lead Contact:**

Jean-Marie Mangin, PhD

Laboratoire Neuroscience Paris Seine

7-9 Quai Saint Bernard

75005 Paris, France

Phone : +33 1 44 27 80 92

Email: jean-marie.mangin@inserm.fr

SUMMARY

In the developing central nervous system, electrical signaling is thought to rely exclusively on differentiating neurons as they acquire the ability to generate and propagate action potentials. Accordingly, neuroepithelial progenitors (NEPs), which give rise to all neurons and glial cells during development, have been reported to remain electrically passive. Here, we investigated the physiological properties of NEPs at the onset of spontaneous neural activity (SNA) initiating motor behavior in mouse embryonic spinal cord. Using patch-clamp recordings, we discovered that spinal NEPs exhibit spontaneous membrane depolarizations during episodes of SNA. These rhythmic depolarizations exhibited a ventral-to-dorsal gradient with the highest amplitude located in the floor-plate, the ventral-most part of the neuroepithelium. Paired-recordings revealed that NEPs are coupled via gap-junctions and form an electrical syncytium. Although other NEPs were electrically passive, we discovered that floor-plate NEPs generated large Na^{+}/Ca^{2+} action potentials. Unlike in neurons, floor-plate action potentials relied primarily on the activation of voltage-gated T-type calcium channels (TTCCs). *In situ* hybridization showed that all 3 known subtypes of TTCCs are predominantly expressed in the floor-plate. During SNA, we found that acetylcholine released by motoneurons rhythmically triggers floor-plate action potentials by acting through nicotinic acetylcholine receptors. Finally, by expressing the genetically encoded calcium indicator GCaMP6f in the floor plate, we demonstrated that neuroepithelial action potentials are associated with calcium waves and propagate along the entire length of the spinal cord. Our work reveals a novel physiological mechanism to generate and propagate electrical signals across a neural structure independently from neurons.

INTRODUCTION

Spontaneous neural activity (SNA) is a hallmark of developing neural networks and has been shown to regulate various developmental processes such as neuronal differentiation, migration, axon guidance and synapse formation[1–4]. Until now, the electrical signals generated during SNA have been found to originate exclusively from differentiating neurons as they acquire the ability to fire action potentials and form their first functional synapses. By contrast, neuroepithelial progenitors (NEPs) – the stem cells of the central nervous system - have never been reported to actively generate or propagate any form of electrical signals, although they can be passively depolarized and/or exhibit calcium events in response to neurotransmitters released by developing neurons[4–11].

SNA was initially described in the embryonic spinal cord where it triggers the first motor rhythmic behavior[12,13], necessary for the proper development of the neuro-muscular and musculo-skeletal systems of vertebrates[14–16]. Spinal SNA starts at midgestation stages - around the 12th day of embryonic development in mice (E12.5) - and is generated autonomously by the ventral spinal cord, before the establishment of sensory inputs from the periphery and descending inputs from the brain. Therefore, SNA is fully preserved in the isolated fetal spinal cord[17,18]. Although its underlying molecular and cellular mechanisms have yet to be fully resolved, spinal SNA has been shown to involve spontaneous waves of electrical activity depolarizing cholinergic motoneurons as well as GABAergic and glutamatergic interneurons along the length of the ventral spinal cord[16–18]. By contrast, the electrophysiological behavior of ventral NEPs remains poorly characterized and they have been assumed to remain electrically passive, as shown in other brain structures. Previous reports indicate that ventral NEPs can exhibit calcium transients during episodes of SNA[11] and that the ventral-most NEPs located in the floor-plate display T-type-like voltage-gated calcium currents[19]. This suggests that spinal NEPs located in the ventral spinal cord could

generate active electrical signals during SNA. To investigate this possibility, we used patch-clamp, optogenetic stimulation and calcium imaging to elucidate the electrophysiological behavior of ventral NEPs during spinal SNA.

RESULTS

We first examined the electrical activity of ventral NEPs using patch-clamp recordings on a preparation of whole spinal cord from E12.5 mouse embryos in the open-book configuration[18,20]. This preparation gave us access to all NEPs lining the central canal while preserving SNA generation (**Figure 1A)**. Five distinct bilateral domains of NEPs are classically identified along the central canal of the ventral spinal cord: p0, p1, p2, pMN and p3 domains (**Figure 1A)**. A sixth unique domain called the floor-plate is located at the base of the spinal cord, joining both sides of the neuroepithelium at the ventral midline. Patch-clamp recordings first revealed that ventral NEPs exhibit spontaneous and rhythmic depolarizations (**Figure 1B & 1G**) at an interval of 183 ± 38 s (N = 32 cells from 23 embryos), similar to the interval previously reported in cholinergic motoneurons during spinal SNA[18]. Strikingly, the amplitude of NEP spontaneous depolarization was not uniform but was inversely correlated to the distance of the recorded NEPs from the ventral midline (**Figure 1C-E**), with the largest depolarization observed in floor-plate NEPs. To determine whether NEP depolarizations were temporally correlated between these different regions, we performed paired recordings between the floor-plate and the neighboring p3 domain. Some of the recorded pairs were also filled with neurobiotin and their molecular identity assessed by post-hoc immunostaining against the transcription factors FOXA2 and NKX2.2 (**Figure 1F**), which are respectively expressed in floor-plate NEPs and in the adjacent p3 neuroepithelial progenitor cells[21]. The average distance between pairs of FP and p3 NEPs filled with neurobiotin was 22 ± 7 µm (N= 6 pairs in 6 embryos). Simultaneous pair recordings demonstrated that rhythmic depolarizations were systematically correlated between FP and p3 NEPs (16/16 events; 5 pairs from 5 embryos; **Figure 1G**), although depolarizations in the p3 domain exhibited significantly smaller amplitudes ($Amplitude_{p3}$ = 22.2 ± 5.5 mV vs $Amplitude_{FP}$ = 55.3 ± 6.8 mV; **Figure 1G and 1H)** with a slight delay ($Delay_{[FP-p3]}$ = 61.2 ± 16.4 ms; **Figure 1G and**

1I) when compared to the floor-plate. The results suggested that these rhythmic depolarizations propagated from the floor-plate to other NEP domains through direct electrical coupling. Indeed, neuroepithelial progenitors are known to be extensively coupled by gap-junctions at this developmental stage[22]. We found that neurobiotin filling via patch pipette often labeled several adjacent cells in the p3 domain (14.7 ± 6.3 cells in p3, N= 6 cells from 6 embryos; **Figure 1F**) as well as in the floor-plate (6.6 ± 2.9 cells in FP, N = 10 cells from 10 embryos; **Figure 1F and 2C**). Depolarizing and hyperpolarizing current steps injected in the floor-plate NEP were also systematically associated with a proportional, albeit much smaller, depolarization or hyperpolarization in the NEP located in the p3 domain (Ratio $_{[p3/FP]}$ = 4.2 ± 1.5 %, N=14 pairs from 14 embryos), showing that they are electrically coupled (**Figure 1J**). Conversely, injecting currents in the NEP located in the p3 domain led to depolarization of the floor-plate cell (Ratio $_{[FP/p3]}$ = 4.6 ± 1.7 %, N = 18 pairs from 18 embryos). Electrical coupling was lost after application of the connexin blocker β18-GA (50µM, paired Wilcoxon test, $p<0.05$; Control Ratio $_{[p3/FP]}$ = 2.9 ± 0.6 % vs β18-GA Ratio $_{[p3/FP]}$ = 0.18 ± 0.07 %, N = 5 pairs from 5 embryos; **Figure 1J and 1K**)[23]. Taken together, our results indicate that NEP depolarizations observed during episodes of SNA originate from the floor-plate and propagate dorsally into the rest of the neuroepithelium, most likely through gap-junctions.

To understand how floor-plate NEPs could exhibit such large and rhythmic depolarizations, we investigated their electrophysiological properties in more detail. Floor-plate cells are easily discriminated from surrounding NEPs by their location at the midline, their thin apical processes and their higher translucency. Identity of the recorded cells were also confirmed by post-hoc immunostaining against the transcription factors FoxA2 and Nkx2.2. All floor-plate cells filled by neurobiotin were found to be $FoxA2^+$ and $Nkx2.2^-$ (N= 10/10 cells from 10 embryos; **Figure 1F and 2C**). Unlike other NEPs that sequentially

generate neurons and glial cells during embryonic development[24], floor-plate NEPs display glial features at an early embryonic stage and have only been shown to generate ependymocytes[25–29]. Indeed, we found that all FoxA2^{+}/Nkx2.2^{-} cells co-expressed the glutamate astrocyte transporter GLAST, a marker for glial progenitors (**Figure S1A-H**) together with the transcription factor Sox2, a marker for neuroepithelial progenitors (**Figure S1I-L**). Floor-plate NEPs had an average membrane resistance of 480 ± 410 MΩ, an average membrane capacitance of 18.3 ± 6.6 pF and an average resting membrane potential of -64.8 ± 9.7 mV (N= 24 cells from 24 embryos). More importantly, we found that floor-plate NEPs had the unique ability to generate action potentials (AP) in response to membrane depolarization (threshold = - 37 ± 3 mV; amplitude = 43.8 ± 14 mV; N= 15 cells from 15 embryos; **Figure 2A**). Unlike most neuronal APs which only rely on voltage-gated sodium channels, floor-plate APs could only be blocked by a combination of TTA-P2 (3 µM), a specific T-type calcium channel blocker, and TTX, a sodium channel blocker (**Figure 2A & 2B**). By contrast, NEPs recorded in the adjacent p3 domain did not exhibit any voltage-dependent responses (N= 24 cells from 24 embryos). During SNA, floor-plate rhythmic depolarizations (amplitude = 54 ± 15 mV; N = 22 cells from 22 embryos; **Figure 1G & 2D**) exhibited a complex and stereotypical time course (**Figure 2E**). These spontaneous events comprised a small initial depolarization (amplitude = 6.9 ± 1.0 mV; half-width = 2.8 ± 1.0 s) followed by an AP exhibiting a biphasic time course comprising first a slow component (amplitude = 18.9 ± 5.5 mV; half-width = 274 ± 57 ms) followed by a fast component (amplitude = 42.4 ± 7.2 mV; half-width = 11.8 ± 3.2 ms; **Figure 2E**). Identical events could be evoked using electrical stimulation (32 mA, 200 µs) placed on the midline, 2 mm rostral to the site of recording (**Figure 2F**). Application of the T-type calcium channel blocker TTA-P2 was sufficient to fully block the biphasic action potential, while the small initial depolarization remained unaffected (N=8/8 cells from 8 embryos). To confirm and further

characterize the expression of T-type calcium channels in the floor-plate, we performed *in situ* hybridization for the 3 known T-type calcium channels (*cacna1g*, *cacna1h, cacna1i*). We found that mRNA coding for T-type calcium channels were all highly and predominantly expressed in the floor-plate (**Figure 2G & 2H**).

Since SNA is dependent on acetylcholine released from motoneurons[17,18], we investigated whether rhythmic floor-plate action potentials were triggered by this neurotransmitter. First, we found that spontaneous rhythmic depolarizations disappeared (N=5/5 cells from 5 embryos; **Figure 3A**) in the presence of the nicotinic acetylcholine receptor (nAChRs) antagonists mecamylamine (50 µM) and d-Tubocurarine (5µM). Evoked floor-plate depolarizations were also completely blocked by the same nAChR antagonists (paired Wilcoxon test, $p<0.01$; N=12 cells from 12 embryos; **Figure 3B & 3C**) as well as by the nAChR antagonist DHβE (5µM; N=4 cells from 4 embryos). By contrast, they remained unaffected by antagonists against $GABA_A$ receptors (Gabazine, 3 µM) and glutamate ionotropic receptors (DL-APV 200 µM and CNQX 20µM), two other neurotransmitters released by spinal interneurons during SNA[17,18] (N=6 cells from 6 embryos; **Figure 3B & 3C**). Conversely, exogenous application of acetylcholine (30 µM) was sufficient to depolarize floor-plate cells (Amplitude = 14.0 ± 2.9 mV; N=9 cells from 9 embryos) and trigger biphasic action potentials (amplitude = 59 ± 7 mV) in a nAChR dependent manner (paired Wilcoxon test, $p<0.05$; N=6 cells from 6 embryos; **Figure 3D & 3E**). Application of the sodium channel blocker TTX together with antagonists of GABA, glutamate and glycine ionotropic receptors had no effect on the depolarization induced by acetylcholine, suggesting that acetylcholine acts directly onto nAChR expressed by floor-plate cells (**Figure 3D & 3E**). We found that TTX suppressed the fast component of the biphasic action potential triggered by acetylcholine (paired Wilcoxon test, $p<0.05$; N=6 cells from 6 embryos; **Figure S2**), demonstrating that it resulted from the activation of voltage-gated sodium channels in floor-plate cells. The slow

component was blocked by TTA-P2 indicating that this resulted from the activation of T-type calcium channels (paired Wilcoxon test, $p<0.05$; N=6 cells from 6 embryos; **Figure S2)**. To confirm that ACh released from motoneurons triggers floor-plate action potentials, we performed optogenetic stimulation using a transgenic mouse model (ChAT:ChR2-YFP) where channelrhodopsin 2 is expressed in cholinergic motoneurons (**Figure 3F-G**). Optogenetic stimulation of cholinergic neurons was sufficient to depolarize and trigger an action potential in floor-plate cells, which could be fully blocked by nAChR antagonists (paired Wilcoxon test, $p<0.05$; N = 5 cells from 5 embryos ; **Figure 3H & 3I)**. To investigate whether cholinergic axons from motoneurons directly contact the floor-plate, we performed immunostaining against vAChT and FoxA2 in coronal sections from E12 HB9:GFP transgenic mice, where GFP is expressed under the promoter for HB9, a homeodomain transcription factor specific of motoneurons at this developmental stage[30,31]. We found the presence of a few HB9:GFP$^+$/vAChT$^+$ axons crossing into the ventral midline (**Figure S3**) where floor-plate basal processes are located. Taken together, our results show that floor-plate action potentials are triggered by the activation of nAChR, most likely in response to acetylcholine released by cholinergic motoneurons during SNA.

Finally, we examined whether and how floor-plate activity could propagate between floor-plate cells along the rostro-caudal axis of the spinal cord. We expressed the genetically encoded calcium indicator GCaMP6f in floor-plate cells using a conditional transgenic approach (GCaMP6floxP x GLASTCreERT2; see Methods). This was achieved by taking advantage of the fact that floor-plate cells are the first neuroepithelial cells to express the glutamate aspartate transporter (GLAST) during spinal cord development[25,26,32] (**Figure 4A** and **Figure S1A-H**). Using this approach, we found that midline floor-plate cells expressing GCaMP6f (**Figure 4A**) generated spontaneous calcium waves at an interval of 176 ± 67 s (N = 31 waves from 10 embryos; **Figure 4B & C** and **Video S1**), similar to the interval observed

for spontaneous floor-plate action potentials. Spontaneous floor-plate calcium waves propagated along the length of the spinal cord and could propagate in either direction. However, rostral to caudal waves initiated in the cervical area were more frequent (67%, 41/61 waves from 10 embryos) than caudal to rostral ones (33%, 20/61 waves) **(Figure S4** and **Video S2)**. Average propagation speed of spontaneous rostro-caudal (2.4 ± 0.9 mm/s) and caudo-rostral floor-plate calcium waves (2.1 ± 1.3 mm/s) were not significantly different (Mann-Whitney test, p=0.12) and their speed was consistent with the propagation speed estimated for SNA waves in motoneurons[17,33].

As observed for floor-plate action potentials, calcium waves could also be consistently triggered using electrical stimulation (32 mA, 200 µs, **Figure 4G, H, J, K** and **Video S3**). Application of the T-type calcium channel blocker TTA-P2 was sufficient to fully block evoked calcium waves (Mann-Whitney test, $p<0.001$, N = 24 waves in 8 embryos; **Figure S5A, S5B & Video S4**), even after increasing the duration of stimulation (32 mA, 1200-1600 µs). The initiation and propagation of evoked calcium waves was also blocked by the application of nAChR antagonists (paired Wilcoxon test, $p<0.001$, N = 6 embryos; **Figure 4G & Video S5**), as observed with floor-plate action potentials (**Figure 3B**). However, increasing stimulation duration (32 mA, 1200-1600 µs) allowed the recovery of floor-plate calcium waves, albeit with a significantly decreased propagation speed of 0.8 ± 0.5 mm/s (paired Wilcoxon test, $p<0.001$, N =31 waves in 6 embryos; **Figure 4G & H, Video S5**). Similarly, patch-clamp experiments showed that after increasing the duration of stimulation in the presence of a cocktail of antagonists to nAChR, GABAaR, GluR and GlyR, the electrical stimulus triggered a delayed biphasic AP without the small initial cholinergic depolarization (N = 4 cells in 4 embryos; **Figure 4I**). This result suggests that, although the initiation and subsequent propagation of floor-plate APs and calcium waves strongly depend on cholinergic transmission, gap-junction coupling between floor-plate cells could also participates in this

propagation (**Figure 2C**). We tested this hypothesis by applying the connexin blocker β18-GA. We found that it either reduced or blocked the propagation of floor-plate calcium waves (paired Wilcoxon test, $p<0.05$, N=18 waves in 6 embryos; **Figure 4J & K, Video S5**) and action potentials (N = 4 cells in 4 embryos; **Figure 4L**) that were evoked in the presence of nAChR antagonists and other neurotransmitter antagonists. Floor-plate calcium waves were also blocked when applying the connexin blocker β18-GA alone (**Figure S5C & D**), confirming that connexins are necessary for calcium wave propagation. The effect of β18-GA could result from the blockade of gap-junction and/or connexin hemichannels[34].

It has previously been shown that the propagation of slow calcium waves between cortical progenitors occurs via ATP signaling acting through high-affinity and slow-acting metabotropic P2YR[9]. By contrast, we found here that the propagation speed of floor plate cells is at least a hundred times faster and primarily rely on nAChRs, T-type calcium channels and connexins. However, there is evidence that ependymal cells derived from the floor-plate express low-affinity but fast-acting ionotropic P2X7 receptors to ATP[35]. We found that floor plate cells only responded to ATP at concentrations above 1 mM, suggesting that they only expressed low-affinity P2X7R (**Figure 5A & 5B**). Indeed, ATP responses were blocked by the competitive antagonist A438079, specific to the low-affinity P2X7R[36] (**Figure 5C & D**). We thus investigated whether P2X7R could actively participate in the propagation of floor plate calcium waves. We found that A438079 significantly reduced the propagation speed of evoked floor-plate calcium waves (**Figure 5E & F**). Since P2X7R have been found to be predominantly expressed by ependymal cells in the postnatal nervous system[37,38], our results are consistent with the ependymal nature of floor plate cells.

Altogether, our results show that the floor-plate of the neuroepithelium possesses the intrinsic ability to generate and propagate electrical signals along the embryonic spinal cord

via the combined activity of nAChRs, voltage-gated T-type calcium channels, voltage-gated sodium channels, connexins and P2X7Rs.

DISCUSSION

Although it has been shown previously that a subpopulation of glial progenitors expressing the proteoglycan NG2 can be induced to generate TTX-sensitive sodium spikes in the postnatal brain[39,40], the neuroepithelial floor-plate is the first example of a non-neuronal structure able to both spontaneously generate and propagate action potentials in the developing central nervous system. Until now, these abilities were considered to be exclusive features of differentiating neurons. Accordingly, the ability to generate and propagate action potentials has been routinely used as a functional assay to confirm the neuronal phenotype of cells during development. In this context, although Ca^{2+}/Na^{+} biphasic action potentials relying on T-type calcium channels are not commonly observed in neurons, their previous discovery in neural cells in the Xenopus embryonic spinal cord[41] and in the mouse fetal hindbrain [42] has been interpreted as an early and transient form of excitability in developing neurons. Instead, we found here that Ca^{2+}/Na^{+} biphasic action potentials are generated in the mouse spinal cord by gliogenic neuroepithelial progenitors located in the floor-plate and that they propagate dorsally in other neuroepithelial cells also engaged into a gliogenic program at this stage[25].

It has previously be shown that T-type voltage-gated currents can be elicited in floor plate cells at later embryonic and perinatal stages in rats[19]. However, only modest depolarizations (10-15 mV) could be elicited in this study when triggering T-type calcium channels by current injection and it was not reported that floor-plate cells could actually generate action potentials. This discrepancy may be explained by the use of coronal slices and/or the absence of voltage-gated sodium channels in floor-plate cells of rats. Indeed, our experiments suggest that the generation of full-fledged action potentials involves the simultaneous activation of numerous cells along the rostro-caudal axis of the floor-plate, as

observed during our calcium imaging experiments. The use of coronal sections may thus have greatly impeded the ability of floor-plate cells to coordinate their activation via gap-junction coupling. The absence of voltage-gated sodium channels would also have impeded the ability of floor-plate cells to generate action potentials in rats. This lack of voltage-gated sodium channels could be the result of the differences in species and/or developmental stages[43].

We found that spontaneous floor-plate calcium waves are initiated at different rostro-caudal location and can propagate in both directions. 2 thirds of the waves are initiated in the cervical area from where they propagate both caudally into the rest of the spinal cord and rostrally towards the brainstem. This latter observation suggests that floor-plate calcium waves may not be restricted to the spinal cord. The last third of the waves propagate in a caudal-to-rostral direction – both at cervical and thoracic level – originating from a yet to be determined caudal location(s). This proportion of waves with a cervical and caudal origin is similar to that previously reported for waves of muscle contractions observed *in vivo* in mouse embryos at the same developmental stage[13]. This suggest that floor-plate activity is likely to be tightly correlated with the first pattern of motoneuron activity and muscle contraction observed *in vivo*.

From an evolutionary point of view, the discovery of an epithelial electrical conduction system in the vertebrate fetal CNS should not come as a complete surprise. Indeed, epithelial and syncytial conduction systems are commonly observed in non-bilaterian animals exhibiting either a “primitive” nervous system, like jellyfish and comb jellies, or in those lacking a nervous system like the glass sponges[44–47]. It has been proposed that the modern neuron-based nervous systems of bilaterians using axonal/chemical synaptic transmission evolved from such epithelial conduction systems coupled electrically by gap-junctions[48]. This evolution would also have been accompanied by a switch from slow voltage-gated calcium channels - inherited from our protist ancestors and still found in the modern

paramecium[49] - to fast voltage-gated sodium channels[48]. Our discovery of a "primitive" electrical conduction system in the neuroepithelium that gives rise to the "modern" nervous system of vertebrates during fetal development could therefore be interpreted as strong evidence supporting this evolutionary scenario.

One may also notice the functional similitude existing between the floor-plate of His and the heart electrical conduction system known as the bundle of His. The bundle of His was discovered by the anatomist and cardiologist Wilhem His, Jr. in 1893[50], five year after his father had described the floor-plate[51]. Both structures act as electrical conduction systems connected by gap junctions able to propagate electrical signals across their respective organs. By showing that these structures not only share the same name but also share similar functional properties, our work reveals that the nervous and cardiac physiologies of vertebrates is more deeply related than previously thought.

Further work will be needed to decipher what function(s) are fulfilled by this non-neuronal electrical conduction system. Although the electrical excitability of floor-plate cells could only be a vestigial property inherited from non-bilaterian ancestors, it is more likely playing a significant role in the development of the spinal cord. Indeed, the energetic cost of generating and propagating electrical signals[52] as well as the redundancy of T-type channel subtypes expressed in the floor-plate point towards having a conserved and significant function. One hypothesis is that floor-plate excitability regulates and coordinates the release of the morphogen Sonic Hedgehog (Shh), required for neural tube patterning, or the expression of axon guidance molecules such as Slit and Netrin. Indeed, recent studies have shown unexpected interactions between early calcium electrical excitability and Shh signalling in the *Xenopus* spinal cord[53,54]. Moreover, T-type channel mutants have recently been identified in a forward genetic screen for neural tube defects in *Ciona intestinalis*[55], suggesting that the electrical gradient established by the floor-plate in the ventral

neuroepithelium could represent a novel morphogenetic mechanism. An additional and non-exclusive hypothesis is that floor-plate action potentials initiated by acetylcholine released by motoneurons during SNA act as a feedback signal to promote the switch from neurogenesis to gliogenesis in ventral neuroepithelial progenitors[25,26] since both events occur around the same developmental stage.

In conclusion, our discovery of the floor-plate of His acting as a non-neuronal electrical conduction system could profoundly change how we conceive of the origin, extent and role of electrical signals during the development of the central nervous system of vertebrates.

ACKNOWLEDGEMENTS

We thank Isabelle Dusart, Marine Robouam, Odile Favière, Goran Fort and Maryse Dardenne for their help in managing mouse colonies; Susanne Bolte, Jean-François Gilles and France Lam for assistance with confocal imaging. We thank Frank Pfrieger for the GLASTCreERT2 mouse line. This study was financially supported by Institut de Recherche sur la Moelle et l'encéphale (JMM), AFM-Telethon (JMM), Agence Nationale de la Recherche (JMM) and Fondation pour la Recherche Médicale (JMM and PL).

AUTHOR CONTRIBUTIONS

K.H.A, G.O and H.L.C. performed and analysed the electrophysiological recordings. K.H. K.H.A, G.O, S.C. and B.L.B. performed and analysed the immunohistochemistry experiments. A.L., K.H.A, L.C. and E.H. performed and analysed calcium imaging experiments. K.H.A, J.B. and A.C. performed and analysed optogenetic experiments. NE. C.S., KK.H.A. and E.H. performed and analysed *in situ* hybridization experiments. C.M. and E.B. managed the animal colony, performed animal genotyping and contributed to immunohistochemistry experiments. J-M.M. supervised the project and wrote the manuscript with P.L., C.S. and E.H..

DECLARATION OF INTERESTS

The authors declare no competing interests.

MAIN-TEXT FIGURE LEGENDS

Figure 1. Neuroepithelial progenitors are spontaneously depolarized during SNA following a ventro-dorsal gradient.

A, Location of the ventral neuroepithelial progenitor domains (p2-p0, pMN, p3, floor-plate) in a coronal view and in open-book configuration. Domains were determined by their distance from the midline (p3 = 30-70 µm; pMN = 70-110 µm; p0-p2 = 110-200 µm). **B,** Spontaneous rhythmic depolarizations recorded in the pMN domain. **C,** Spontaneous depolarizations recorded separately in the p0-p2, pMN and p3 domains. **D,** Average amplitude of spontaneous depolarizations recorded in different NEP domains. **E,** Drawing illustrating the depolarization gradient observed in the ventral neuroepithelium. **F,** Pair of FP and p3 NEPs filled with neurobiotin and stained against FoxA2 and Nkx2.2. Recorded cells are indicated by yellow arrowheads. **G,** Spontaneous rhythmic depolarizations simultaneously recorded in the FP and a p3 domain and close up of a simultaneous depolarization. **H**, Amplitude of depolarizations recorded simultaneously in the p3 and floor-plate NEPs (N= 16 depolarizations; 5 pairs from 5 embryos). **I**, Delay between the peak of depolarizations in p3 and floor-plate NEPs. **J,** Current injection (top traces) in FP or p3 NEPs show electrical symmetrical electrical coupling (bottom traces) which is lost after application of the connexin blocker β18-GA. **K,** Effect of β18-GA on electrical coupling (paired Wilcoxon test; * $p<0.05$: N= 5 pairs from 5 embryos).

Figure 2. Floor-plate neuroepithelial progenitors generate rhythmic action potentials during spinal SNA.

A, Responses of a FP cell to current steps in control conditions, after application of the T-type calcium channel blocker TTA-P2 (3 µM) and subsequent addition of the sodium channel blocker TTX (1 µM). **B**, Maximal amplitude of the spike triggered in each pharmacological

condition (N = 15 cells from 15 embryos). **C,** FP cell (yellow asterisk) filled with neurobiotin and immuno-stained against FoxA2 and Nkx2.2. **D,** Spontaneous rhythmic depolarization recorded in a FP cells. **E,** Magnified view of a spontaneous depolarization revealing the presence of three distinct components: a small initial depolarization (1) and a biphasic action potential (AP, grey area magnified in insert) composed of a slow (2) and fast component (3). **F,** Depolarization and biphasic AP evoked by electrical stimulation. Application of TTA-P2 (3 µM) blocked the biphasic AP while the small initial depolarization remained unaffected (N = 8 cells from 8 embryos, paired Wilcoxon text; ** $p<0.01$). **G,** *In situ* hybridization showing the location of mRNA transcripts for the 3 known sub-types of T-type channels (*cacna1g, cacna1h, cacna1i*) in coronal sections of E12.5 mouse embryos. **H,** *In situ* hybridization showing location of mRNA transcripts for *cacna1g* in open-book configuration. See also Figure S1 and S2.

Figure 3. Floor-plate biphasic action potentials are triggered by the activation of nicotinic acetylcholine receptors.

A, Rhythmic spontaneous floor-plate action potentials are blocked after addition of the nAChR antagonists Mecamylamine (50 µM) and d-Tubocurarine (5 µM). **B,** FP action potential evoked by electrical stimulation in control condition, after addition of the nAChR antagonists and after addition of antagonists against ionotropic receptor for GABA (Gabazine 3 µM) and glutamate (DL-APV 200 µM and CNQX 20 µM). **C**, Total depolarization amplitude in control conditions and after addition of nAChR antagonists (N = 12 cells from 12 embryos, paired Wilcoxon text, ** = $p<0.01$) as well as in presence of antagonists against ionotropic receptor for GABA and glutamate (N = 6 cells from 6 embryos; n.s. = non-significant) **D,** FP action potential can be evoked by local application of 30 µM ACh, even in the presence of TTX (1 µM) and antagonists to AMPA/Kainate glutamate receptor (CNQX 10

μM), NMDA glutamate receptor (DL-APV 200 μM), $GABA_A$ receptor (Gabazine 3 μM) and glycine receptor (strychnine 1 μM). Floor-plate action potential evoked by ACh were blocked by the addition of nAChR antagonists. **E,** Slow depolarization amplitude induced by 30 μM Ach (arrows in d) in each condition (N = 6 cells from 6 embryos, paired Wilcoxon text; ** $p<0.01$, n.s. non-significant). **F,** Coronal section from a ChAT:ChR2-YFP mouse embryo showing the expression of Channelrhodopsin2-YFP fusion protein in cholinergic motoneurons located in the ventro-dorsal horns and labelled with the vesicular acetylcholine transporter vAChT. All cell nuclei were labelled using DAPI. **G,** Action potential triggered in a ChAT:ChR2-YFP^+ motoneuron in response to a 300 ms blue light stimulus delivered through a optic fiber cannula (470 nm, 400μm-diameter cannula, output power: 9-18 mW). **H,** FP response recorded in a ChAT:ChR2-YFP^+ fetal spinal cord showing how a 4 s blue light stimulus (470 nm, 400μm-diameter cannula, output power: 9-18 mW) could evoke a slow cholinergic depolarization and trigger a biphasic action potential that were blocked by the addition of nAChR antagonists. **I,** Total depolarization amplitude evoked by a blue light stimulus in control conditions and after application of nAChR antagonists (N = 5 cells from 5 embryos; paired Wilcoxon text; * $p<0.05$). See also Figure S2 and S3.

Figure 4. Floor-plate action potentials are associated with calcium waves and propagate along the length of the spinal cord.

A, GCaMP6 expression in $FoxA2^+/Nkx2.2^-$ cells. **B,** Rhythmic spontaneous calcium events are observed in FP cells expressing GCaMP6. Asterisk indicates the event represented in d. **C,** Intervals between spontaneous calcium events (Mann-whitney test; n.s. non-significant). **D,** Rostro-caudal propagation of calcium waves in FP cells visualized in the thoracic region. Dotted boxes represent the region of interest used to calculate propagation speeds. **E**, Variation of intensity of fluorescence (dF/F) over time in the 3 regions of interest indicated in

E. Dotted lines mark the onset of the calcium signals in region i (left) and iii (right). **F,** Propagation speed of FP calcium waves (Mann-whitney test; n.s. = non-significant). **G**, Color-coded calcium waves evoked by rostral electrical stimulation (32 mA, 200 µs) in control condition, after application of antagonists to nAChR and subsequent increase of stimulation intensity (32 mA, 1200 µs). Time after stimulation is coded in distinct colors as indicated in the scale at the bottom. **H**, Propagation speed of evoked FP calcium waves in different pharmacological conditions (Mann-whitney test; *** $p<0.001$). **I,** Evoked depolarization in control condition, after application of a cocktail of antagonists to nAChR, $GABA_AR$, iGluR and GlyR and subsequent increase of stimulation intensity. **J,** Color-coded calcium waves evoked by increased electrical stimulation (32 mA, 1200 µs) in the presence of antagonists to nAChR and after addition of the connexin blocker β18-GA. **K**, Propagation speed before and after addition of antagonists to nAChR and gap junction blockers (Mann-whitney test;* $p<0.05$). **L**, Evoked depolarization in the presence of a cocktail of antagonists to nAChR, $GABA_AR$, iGluR and GlyR and after subsequent addition of the connexin blocker β18-GA. See also Figure S4, S5 and Video S1-S5.

Figure 5. P2X7R are expressed by floor-plate cells and participate to calcium wave propagation.

A, Responses of a floor-plate cell to different concentration of ATP. **B**, Slow depolarization amplitude (arrows in a) induced by different concentration of ATP (N = 7 cells from 7 embryos, paired Wilcoxon test; n.s. non-significant). **C**, FP response to 3 mM ATP in control conditions, in the presence of a P2X7R antagonist (30 µM of A438079) and after washout. **D**, Slow depolarization amplitude (arrows in c) induced by 3 mM ATP application in each condition (N = 6 cells from 6 embryos, paired Wilcoxon test; *** $p<0.001$). **e**, Color-coded calcium waves evoked by rostral electrical stimulation (32 mA, 200 µs) in control condition,

after application of a P2X7R antagonist (30 μM of A438079) and after washout. **f**, Propagation speed of evoked FP calcium waves in control conditions, after addition of P2X7R antagonist and washout (Mann-whitney test; * $p<0.05$, *** $p<0.001$). See also Figure S5.

STAR METHODS

Resource availability

Lead contact

Further information and requests for resources and reagents should be directed to and will be fulfilled by the lead contact, jean-Marie Mangin (jean-marie.mangin@inserm.fr)

Materials Availability

This study did not generate new unique reagents.

Data and code availability

- This study did not generate any unique dataset.
- This study did not generate any original code.
- All data needed to evaluate the conclusions are present in this paper and/or the supplemental information. Any additional information required to reanalyze the data reported in this paper is available from the lead contact upon request.

Experimental models and subject details

All experiments were performed in accordance with European Community guiding principles on the care and use of animals (86/609/CEE, CE Off J no. L358, 18 December, 1986), French decree no. 97/748 of October 19, 1987 (J Off République Française, 20 October, 1987, pp. 12245–12248) and recommendations from the CNRS. All efforts were made to minimize the suffering of animals. In order to maximize litter size, experiments were performed on E12.5 mouse embryos obtained by crossing C57BL/6 males with females from a Swiss strain. For optogenetic stimulation of cholinergic motoneurons, we used C57BL/6

breeding male mice expressing a BAC transgene containing a Channelrhodopsin2-EYFP sequence driven by a Choline Acetyl Transferase (ChAT) promoter (ChAT-ChR2–EYFP, The Jackson Laboratory, USA, https://www.jax.org/strain/014546)[56]. We used C57BL/6 mice expressing a Hb9-GFP transgene [30] to visualize motoneuron axons crossing into the floor-plate. For calcium imaging of floor-plate cells, we used C57BL/6 breeding male mice expressing a genetically encoded floxed Calcium indicator GCaMP6f (Ai95, The Jackson Laboratory, USA, https://www.jax.org/strain/028865), crossed with Swiss female mice expressing a tamoxifen-inducible Cre recombinase under the control of the glutamate aspartate transporter promoter (GLASTCreERT2, gift from Dr Frank Pfrieger)[57]. Cre recombination was induced by oral gavage of pregnant mice with 5 mg of tamoxifen (Sigma-Aldrich, France, T-5648) at embryonic days E10.5 and E11.5[58]. Tamoxifen was dissolved in corn oil at 37°C for several hours to prepare 20 mg/mL solution[59].

Method details

In situ RNA hybridization staining

Mouse embryos were fixed in 3.7% paraformaldehyde (PFA) in PBS overnight at 4°C. Tissues were then sectioned at 60–80 µm using a vibratome (Microm, France). In all experiments, sections were performed at the cervico/brachial level. In situ hybridization (ISH) was performed on vibratome sections automatically (InsituPro, Intavis, Germany) using the whole-mount ISH as previously reported[60]. Digoxigenin (DIG)-labeled antisense RNA probes were synthesized using T3 polymerase from the following I.M.A.G.E. Consortium cDNA Clones[61]: *cacna1g*, (ID 6410519); *cacna1h* (ID 6820407) and *cacna1i* (ID 6825802). RNA labeled probes were detected by an alkaline-phosphatase coupled antibody (Roche Diagnostics), and NBT/BCIP (nitroblue tetrazolium/5-bromo-4-chloro-3-indolyl phosphate) were used as a chromogenic substrate for the alkaline phosphatase (Boehringer Mannheim,

Germany). Stained sections were digitized and analyzed using Zeiss acquisition software (Zeiss, Germany).

Isolated embryonic spinal cord preparation

E12.5 embryonic mouse spinal cords were dissected as previously described[18,20]. Briefly, pregnant mice were killed using a lethal dose of CO_2 followed by cervical dislocation. Mice embryos of both sexes were dissected and whole spinal cord were left to recover for at least 30 min at 32˚C in artificial cerebrospinal fluid (ACSF) containing 125 mM NaCl, 25mM NaHCO3, 11 mM Glucose, 3 mM KCl, 1 mM MgCl2, 2 mM CaCl2, and 1 mM NaH2PO4 (pH 7.3; 307 mOsm) continuously bubbled with 95% O_2 – 5% CO_2 gas, before being recorded or imaged. For ChAT-ChR2-EYFP and GCaMP6floxP x GLASTCreERT2 transgenic embryos, their tails were cut and observed under a fluorescent stereo-microscope (Leica MZ FLIII) to identify positive embryos for EYFP and GCaMP6, respectively.

Patch-clamp recordings

Isolated spinal cords were placed in open-book configuration in a recording chamber under a nylon holding grid and continuously perfused (2 ml/min) at room temperature with the oxygenated ACSF described above. In contrast to previous studies[18,20], the orientation of open-book spinal cord was inverted so that the neuroepithelial layer was facing upward. Whole-cell voltage-clamp recordings of floor-plate cells and other neuroepithelial progenitors were performed under direct visualization using an infrared-sensitive CCD video camera. In addition to their location at the midline, floor-plate cells were distinguished from surrounding neuroepithelial progenitors based on their smaller apical process and their higher translucency when using brightfield microscopy. To confirm their identity, some recorded cells were filled with neurobiotin (1 mg/ml, Vector labs, USA) and revealed in combination with FoxA2 and

Nkx2.2 immunostaining. Whole-cell patch-clamp electrodes were pulled from thick-wall borosilicate glass using a Brown-Flaming puller (P97, Sutter Instrument, USA). The tip of the electrode was fire-polished using a microforge (MF-830, Narishige, Japan). Patch-clamp electrodes had tip resistances comprised between 4 and 7 MΩ. Electrodes were filled with an intracellular solution containing either (in mM): 96.4 K^+-methanesulfonate, 33.6 KCl, 4 MgCl2, 4 Na_2ATP, 0.3 Na_3GTP, 10 EGTA, and 10 HEPES or 100 K^+-gluconate, 34 KCl, 0.5 EGTA, 10 HEPES, 4 $MgCl_2$, 4 Na_2ATP (pH 7.2; 290 mOsm). In both solutions, the theoretical equilibrium potential for chloride ions (ECl) was -30 mV, while cation reversal potential (Ecat) was 0 mV. Signals were recorded with a low-pass filtered at 4 kHz using a Multiclamp 700B amplifier (Molecular Devices, USA) and digitized at 20 kHz using a Digi-data 1440A interface coupled to pClamp 10.5 software (Molecular Devices, USA) running on a PC computer. Cells exhibiting an average resting membrane potential above -50 mV (I=0 pA) were discarded from further analysis.

Electrical and optogenetic stimulation

For electrical stimulations experiments, we used bipolar platinum electrodes (FHC, USA) placed 2 mm rostrally to the recording site onto the midline. For optogenetic stimulation of ChAT-ChR2 we used a 400 µm diameter optical fiber coupled with a 470 LED (Thorlabs, Germany) and centered onto the recording site. Electrical and optogenetic stimulations were performed at a low frequency (0.005 Hz, 1 stimulation every 180 s) in order to evoke a stable cholinergic response.

Calcium imaging

Isolated spinal cords were placed in open-book configuration under a nylon holding grid in a recording chamber and continuously perfused (2mL/min) with the same oxygenated

ACSF described above. Recombined fluorescent cells were observed under an epifluorescence microscope BX51W1 (Olympus) with a 470-515nm fluorescent excitation light to confirm GCaMP6f expression in the floor-plate. Time-lapse imaging was performed using either an Orca Flash4.0 (Hamamatsu, Japan) or Orca 03G (Hamamatsu, Japan) camera and recorded using the HC Image Live software (Hamamatsu, Japan) at an acquisition frequency of 5 or 10Hz with an exposure time of 200 ms and 100 ms, respectively. Images were encoded using a 256x256 or 512x512 pixel resolution and 16-bit grey scale. Time-lapse images were analyzed using the ImageJ software (National Institute of Health, USA). Signals were either extracted by subtracting each frame from the one following it (Figure 4g & 4i) or by subtracting an average of 10 frames preceding the onset of an event (Figure 4d, Supplementary Figure 3 and Supplementary videos 1-5). To measure the propagation speed, we pinpointed three regions of interest on the midline and measured the delays necessary to reach half-peak between each region of interest and averaged them. Intensity of signals (dF/F) were measured by dividing the peak amplitude of the events by the baseline value in raw images.

Pharmacological agents

In most experiments, drugs were applied via the bath perfusion system. Typically, the effect of drugs reached equilibrium within 3 to 5 minutes. For acetylcholine application, we used a 0.5 mm diameter quartz tubing positioned 50 µm away from the recording area under direct visual control. Typically, response to acetylcholine reached equilibrium a few seconds (6 sec) after solution switch. The quartz tubing was connected using a manifold to six solenoid valves linked with six reservoirs. Solutions were gravity-fed into the quartz tubing. Drug application was controlled using a VC-8 valve controller (Warner Instruments, USA). At least 3 events were recorded in each condition after waiting 5 min for drugs to act. The

following pharmacological agents were used: Acetylcholine chloride (30 µM, Sigma-Aldrich, Germany), TTX (1 µM, Alomone Labs, Israel), gabazine (3 µM, Tocris, USA), CNQX Disodium (20 µM, Tocris, USA), DL-APV (200 µM, Tocris, USA), Mecamylamine hydrochloride (100 µM, Tocris, USA), D-tubocurarine chloride (10 µM, Tocris, USA), 18- β glycyrrhetinic acid (50 µM, Sigma-Aldrich, Germany), TTA-P2 (3µM, Alomone, Israel), A438079 (30 µM, Tocris, USA) and DHβE (5 µM, Tocris, USA). All drugs were dissolved at final concentration in ACSF.

Immunohistochemistry

E12.5 embryos or whole embryonic spinal cord were immersion-fixed in phosphate buffer saline (PBS) with 4% PFA freshly prepared in PBS (pH 7.4) for 1 h at 4°C. Embryos were then rinsed with PBS and cryoprotected in PBS-15% sucrose at 4°C for 24 h and then in PBS-30% sucrose at 4°C for 24 h. Embryos were embedded in OCT medium (VWR, USA) and quickly frozen. Serial sections 20 µm thick were collected onto slides using a cryostat (Leica, Wetzlar, Germany) and stored at -80°C until immunohistochemical studies. For immunostaining, slides and whole spinal cord were washed in PBS, incubated in NH_4Cl (50 mM) diluted in PBS for 20 min and then permeabilized for 30 min in a blocking solution (10% goat serum in PBS) with 0.2% Triton X-100. They were incubated overnight at 4°C with the primary antibodies, which were diluted in the 0.2% Triton X-100 blocking solution. Slides or whole spinal cords were then washed in PBS and incubated for 2h at room temperature in the appropriate secondary antibodies (diluted at 1/1000 in the 0.2% Triton X-100 blocking solution). The following primary antibodies were used: a mouse monoclonal anti-HNF-3β/FoxA2 (H-4) antibody sc-374376 (1:300, Santa Cruz Biotechnology, USA), a mouse monoclonal anti-Nkx2.2 antibody 74.5A5 (1:600, Developmental Studies Hybridoma Bank, USA), a guinea-pig polyclonal anti-EAAT1/GLAST antibody 250 114 (1:1000,

Synaptic System, Germany), a mouse monoclonal anti-Sox2 (E-4) antibody sc-365823 (1:500, Santa Cruz Biotechnology, USA), a rabbit polyclonal anti-vAChT antibody 139 103 (1:1000, Synaptic System, Germany) and a rabbit polyclonal anti-GFP antibody A-11122 (1:1000, Thermo Fisher Scientific, USA). Alexa Fluor 405-, 488-, or 594- and 647-conjugated secondary antibodies (1/1000; Invitrogen, USA) were used to detect mouse monoclonal, guinea pig and rabbit polyclonal primary antibodies. After washing in PBS, slides or whole spinal cords were dried and mounted in Mowiol medium (Millipore, USA).

Confocal microscopy

Once mounted, immunostained sections were imaged using a SP5 confocal microscope (Leica, Germany) using a 20X oil-immersion objective with a numerical aperture of 1.25, as well as with a 63X oil-immersion objective with a numerical aperture of 1.32 and a 1X digital zoom magnification. Serial optical sections were acquired with a Z-step of 3 µm (20X) and 0.78 µm (63X). Images (1024 X 1024; 8 to16 bit grayscale) were acquired using Leica software LAS-AF and analyzed using ImageJ (National Institutes of Health, USA). Colocalization with neurobiotin staining was assessed in three axes using a single confocal slice and x and y orthogonal views of the stack (ImageJ 1.5). To quantify the number of cells filled by neurobiotin after patch-clamp recording in the floor-plate and/or p3 domain, neurobiotin staining was combined with antibody staining against FoxA2, Nkx2.2 and DAPI. FoxA2 and Nkx2.2 are respectively labelling the nucleus of NEPs in the floor-plate and the p3 domain. No neurobiotin staining was found to colocalize with a DAPI stained nucleus without being also positive for either FoxA2 or Nkx2.2. DAPI is not shown for clarity in merged confocal images.

Quantification and statistical analysis

Each protocol was triplicated in each cell (patch-clamp experiments) and embryos (calcium imaging experiments). Statistical comparisons for electrophysiological recordings and calcium imaging parameters were conducted using GraphPad Prism 8 (GraphPad Software, USA) by performing non-parametric Wilcoxon-Mann-Whitney U tests (calcium imaging experiments) and Wilcoxon signed rank test for paired samples (patch-clamp experiments). We determined that statistical significance was obtained when the one-tailed p-value was <0.05.

REFERENCES

1. Moody, W.J., and Bosma, M.M. (2005). Ion channel development, spontaneous activity, and activity-dependent development in nerve and muscle cells. Physiol. Rev. *85*, 883–941.

2. Spitzer, N.C. (2006). Electrical activity in early neuronal development. Nature *444*, 707–712.

3. Blankenship, A.G., and Feller, M.B. (2010). Mechanisms underlying spontaneous patterned activity in developing neural circuits. Nat. Rev. Neurosci. *11*, 18–29.

4. Kirischuk, S., Sinning, A., Blanquie, O., Yang, J.W., Luhmann, H.J., and Kilb, W. (2017). Modulation of neocortical development by early neuronal activity: Physiology and pathophysiology. Front. Cell. Neurosci. *11*.

5. Corlew, R., Bosma, M.M., and Moody, W.J. (2004). Spontaneous, synchronous electrical activity in neonatal mouse cortical neurones. J. Physiol. *560*, 377–390.

6. Vitali, I., Fièvre, S., Telley, L., Oberst, P., Bariselli, S., Frangeul, L., Baumann, N., McMahon, J.J., Klingler, E., Bocchi, R., et al. (2018). Progenitor Hyperpolarization Regulates the Sequential Generation of Neuronal Subtypes in the Developing Neocortex. Cell *174*, 1264-1276.e15.

7. LoTurco, J.J., Owens, D.F., Heath, M.J.S., Davis, M.B.E., and Kriegstein, A.R. (1995). GABA and glutamate depolarize cortical progenitor cells and inhibit DNA synthesis. Neuron *15*, 1287–1298.

8. Noctor, S.C., Flint, A.C., Weissman, T.A., Wong, W.S., Clinton, B.K., and Kriegstein, A.R. (2002). Dividing precursor cells of the embryonic cortical ventricular zone have

morphological and molecular characteristics of radial glia. J. Neurosci. *22*, 3161–3173.

9. Weissman, T.A., Riquelme, P.A., Ivic, L., Flint, A.C., and Kriegstein, A.R. (2004). Calcium waves propagate through radial glial cells and modulate proliferation in the developing neocortex. Neuron *43*, 647–661.

10. Rosa, J.M., Bos, R., Sack, G.S., Fortuny, C., Agarwal, A., Bergles, D.E., Flannery, J.G., and Feller, M.B. (2015). Neuron-glia signaling in developing retina mediated by neurotransmitter spillover. Elife *4*.

11. Wang, S., Polo-Parada, L., and Landmesser, L.T. (2009). Characterization of Rhythmic Ca2+ Transients in Early Embryonic Chick Motoneurons: Ca2+ Sources and Effects of Altered Activation of Transmitter Receptors. J. Neurosci. *29*, 15232–15244.

12. Hamburger, V., and Balaban, M. (1963). Observations and experiments on spontaneous rhythmical behavior in the chick embryo. Dev. Biol. *7*, 533–545.

13. Suzue, T., and Shinoda, Y. (1999). Highly reproducible spatiotemporal patterns of mammalian embryonic movements at the developmental stage of the earliest spontaneous motility. Eur. J. Neurosci. *11*, 2697–2710.

14. Landmesser, L.T. (2018). General principles of spinal motor circuit development: early contributions from research on avian embryos. Int. J. Dev. Biol. *62*, 235–243.

15. Shwartz, Y., Blitz, E., and Zelzer, E. (2013). One load to rule them all: Mechanical control of the musculoskeletal system in development and aging. Differentiation *86*, 104–111.

16. Hanson, M.G., Milner, L.D., and Landmesser, L.T. (2008). Spontaneous rhythmic activity in early chick spinal cord influences distinct motor axon pathfinding decisions.

Brain Res. Rev. *57*, 77–85.

17. Hanson, M.G., and Landmesser, L.T. (2003). Characterization of the circuits that generate spontaneous episodes of activity in the early embryonic mouse spinal cord. J. Neurosci. *23*, 587–600.

18. Czarnecki, A., Le Corronc, H., Rigato, C., Le Bras, B., Couraud, F., Scain, A.-L., Allain, A.-E., Mouffle, C., Bullier, E., Mangin, J.-M., et al. (2014). Acetylcholine controls GABA-, glutamate-, and glycine- dependent giant depolarizing potentials that govern spontaneous motoneuron activity at the onset of synaptogenesis in the mouse embryonic spinal cord. J. Neurosci. *34*.

19. Frischknecht, F., and Randall, A.D. (1998). Voltage- and ligand-gated ion channels in floor plate neuroepithelia of the rat. Neuroscience *85*, 1135–49.

20. Osterstock, G., Le Bras, B., Arulkandarajah, K.H., Le Corronc, H., Czarnecki, A., Mouffle, C., Bullier, E., Legendre, P., and Mangin, J.-M. (2018). Axoglial synapses are formed onto pioneer oligodendrocyte precursor cells at the onset of spinal cord gliogenesis. Glia.

21. Lupo, G., Harris, W.A., and Lewis, K.E. (2006). Mechanisms of ventral patterning in the vertebrate nervous system. Nat. Rev. Neurosci. *7*, 103–114.

22. Bittman, K.S., Panzer, J.A., and Balice-Gordon, R.J. (2004). Patterns of cell-cell coupling in embryonic spinal cord studied via ballistic delivery of gap-junction-permeable dyes. J. Comp. Neurol. *477*, 273–285.

23. Rozental, R., Srinivas, M., and Spray, D.C. (2001). How to close a gap junction channel. Efficacies and potencies of uncoupling agents. Methods Mol. Biol. *154*, 447–476.

24. Rowitch, D.H. (2004). Glial specification in the vertebrate neural tube. Nat. Rev. Neurosci. *5*, 409–19.

25. Deneen, B., Ho, R., Lukaszewicz, A., Hochstim, C.J., Gronostajski, R.M., and Anderson, D.J. (2006). The Transcription Factor NFIA Controls the Onset of Gliogenesis in the Developing Spinal Cord. Neuron *52*, 953–968.

26. Barry, D., and McDermott, H. (2005). Differentiation of radial glia from radial precursor cells and transformation into astrocytes in the developing rat spinal cord. Glia *50*, 187–197.

27. Cañizares, M.A., Albors, A.R., Singer, G., Suttie, N., Gorkic, M., Felts, P., and Storey, K.G. (2019). Multiple steps characterise ventricular layer attrition to form the ependymal cell lining of the adult mouse spinal cord central canal. J. Anat.

28. Khazanov, S., Paz, Y., Hefetz, A., Gonzales, B.J., Netser, Y., Mansour, A.A.F., and Ben-Arie, N. (2017). Floor plate descendants in the ependyma of the adult mouse Central Nervous System. Int. J. Dev. Biol. *61*, 257–265.

29. Mirzadeh, Z., Kusne, Y., Duran-Moreno, M., Cabrales, E., Gil-Perotin, S., Ortiz, C., Chen, B., Garcia-Verdugo, J.M., Sanai, N., and Alvarez-Buylla, A. (2017). Bi- and uniciliated ependymal cells define continuous floor-plate-derived tanycytic territories. Nat. Commun. *8*.

30. Wichterle, H., Lieberam, I., Porter, J.A., and Jessell, T.M. (2002). Directed differentiation of embryonic stem cells into motor neurons. Cell *110*, 385–397.

31. Le Bras, B., Fréal, A., Czarnecki, A., Legendre, P., Bullier, E., Komada, M., Brophy, P.J., Davenne, M., and Couraud, F. (2014). In vivo assembly of the axon initial segment in motor neurons. Brain Struct. Funct. *219*, 1433–1450.

32. Shibata, T., Yamada, K., Watanabe, M., Ikenaka, K., Wada, K., Tanaka, K., and Inoue, Y. (1997). Glutamate transporter GLAST is expressed in the radial glia-astrocyte lineage of developing mouse spinal cord. J. Neurosci. *17*, 9212–9.

33. Scain, A.-L., Le Corronc, H., Allain, A.-E., Muller, E., Rigo, J.-M., Meyrand, P., Branchereau, P., and Legendre, P. (2010). Glycine release from radial cells modulates the spontaneous activity and its propagation during early spinal cord development. J. Neurosci. *30*, 390–403.

34. J, W., M, M., S, C.Y., and M, V. (2017). Inhibitors of connexin and pannexin channels as potential therapeutics. Pharmacol. Ther. *180*, 144–160.

35. Marichal, N., Fabbiani, G., Trujillo-Cenóz, O., and Russo, R.E. (2016). Purinergic signalling in a latent stem cell niche of the rat spinal cord. Purinergic Signal. *12*, 331–341.

36. Donnelly-Roberts, D.L., and Jarvis, M.F. (2007). Discovery of P2X 7 receptor-selective antagonists offers new insights into P2X 7 receptor function and indicates a role in chronic pain states. Br. J. Pharmacol. *151*, 571–579.

37. Collo, G., Neidhart, S., Kawashima, E., Kosco-Vilbois, M., North, R.A., and Buell, G. (1997). Tissue distribution of the P2X7 receptor. Neuropharmacology *36*, 1277–1283.

38. Genzen, J.R., Platel, J.C., Rubio, M.E., and Bordey, A. (2009). Ependymal cells along the lateral ventricle express functional P2X7 receptors. Purinergic Signal. *5*, 299–307.

39. Chittajallu, R., Aguirre, A., and Gallo, V. (2004). NG2-positive cells in the mouse white and grey matter display distinct physiological properties. J. Physiol. *561*, 109–122.

40. Káradóttir, R., Hamilton, N.B., Bakiri, Y., and Attwell, D. (2008). Spiking and nonspiking classes of oligodendrocyte precursor glia in CNS white matter. Nat. Neurosci. *11*, 450–456.

41. Gu, X., Olson, E.C., and Spitzer, N.C. (1994). Spontaneous neuronal calcium spikes and waves during early differentiation. J. Neurosci. *14*, 6325–6335.

42. Moruzzi, A.M., Abedini, N.C., Hansen, M.A., Olson, J.E., and Bosma, M.M. (2009). Differential expression of membrane conductances underlies spontaneous event initiation by rostral midline neurons in the embryonic mouse hindbrain. J. Physiol. *587*, 5081–93.

43. Placzek, M., and Briscoe, J. (2005). The floor plate: Multiple cells, multiple signals. Nat. Rev. Neurosci. *6*, 230–240.

44. Meech, R.W. (2015). Electrogenesis in the lower Metazoa and implications for neuronal integration. J. Exp. Biol. *218*, 537–550.

45. Mackie, G.O. (1970). Neuroid conduction and the evolution of conducting tissues. Q. Rev. Biol. *45*, 319–332.

46. Anderson, P.A.V. (1980). Epithelial conduction: Its properties and functions. Prog. Neurobiol. *15*, 161–203.

47. Leys, S.P., Mackie, G.O., and Reiswig, H.M. (2007). The Biology of Glass Sponges. Adv. Mar. Biol. *52*, 1–145.

48. Castelfranco, A.M., and Hartline, D.K. (2016). Evolution of rapid nerve conduction. Brain Res. *1641*, 11–33.

49. Eckert, R., Naitoh, Y., and Friedman, K. (1972). Sensory mechanisms in Paramecium.

I. Two components of the electric response to mechanical stimulation of the anterior surface. J. Exp. Biol. *56*, 683–694.

50. Bast, T.H., and Gardner, W.D. (1949). Wilhelm His, Jr. and the Bundle of His. J. Hist. Med. Allied Sci. *IV*, 170–187.

51. Kingsbury, B.F. (1920). The extent of the floor-plate of his and its significance. J. Comp. Neurol. *32*, 113–135.

52. Attwell, D., and Laughlin, S.B. (2001). An energy budget for signaling in the grey matter of the brain. J. Cereb. Blood Flow Metab. *21*, 1133–1145.

53. Belgacem, Y.H., Borodinsky, L.N., and Stevens, C.F. (2015). Inversion of Sonic hedgehog action on its canonical pathway by electrical activity. Proc. Natl. Acad. Sci. U. S. A. *112*, 4140–4145.

54. Borodinsky, L.N., and Belgacem, Y.H. (2016). Crosstalk among electrical activity, trophic factors and morphogenetic proteins in the regulation of neurotransmitter phenotype specification. J. Chem. Neuroanat. *73*, 3–8.

55. Abdul-Wajid, S., Morales-Diaz, H., Khairallah, S.M., and Smith, W.C. (2015). T-type Calcium Channel Regulation of Neural Tube Closure and EphrinA/EPHA Expression. Cell Rep. *13*, 829–839.

56. Zhao, S., Ting, J.T., Atallah, H.E., Qiu, L., Tan, J., Gloss, B., Augustine, G.J., Deisseroth, K., Luo, M., Graybiel, A.M., et al. (2011). Cell type-specific channelrhodopsin-2 transgenic mice for optogenetic dissection of neural circuitry function. Nat. Methods *8*, 745–755.

57. Slezak, M., Göritz, C., Niemiec, A., Frisén, J., Chambon, P., Metzger, D., and Pfrieger,

F.W. (2007). Transgenic mice for conditional gene manipulation in astroglial cells. Glia *55*, 1565–1576.

58. Eon, J.P., Sun, X., Nichol, P., Saijoh, Y., Martin, J.F., and Moon, A.M. (2008). System for tamoxifen-inducible expression of Cre-recombinase from the Foxa2 locus in mice. Dev. Dyn. *237*, 447–453.

59. Zervas, M., Millet, S., Ahn, S., and Joyner, A.L. (2004). Cell behaviors and genetic lineages of the mesencephalon and rhombomere 1. Neuron *43*, 345–357.

60. Touahri, Y., Escalas, N., Benazeraf, B., Cochard, P., Danesin, C., and Soula, C. (2012). Sulfatase 1 promotes the motor neuron-to-oligodendrocyte fate switch by activating Shh signaling in Olig2 progenitors of the embryonic ventral spinal cord. J. Neurosci. *32*, 18018–18034.

61. Lennon, G., Auffray, C., Polymeropoulos, M., and Soares, M.B. (1996). The I.M.A.G.E consortium: An integrated molecular analysis of genomes and their expression. Genomics *33*, 151–152.

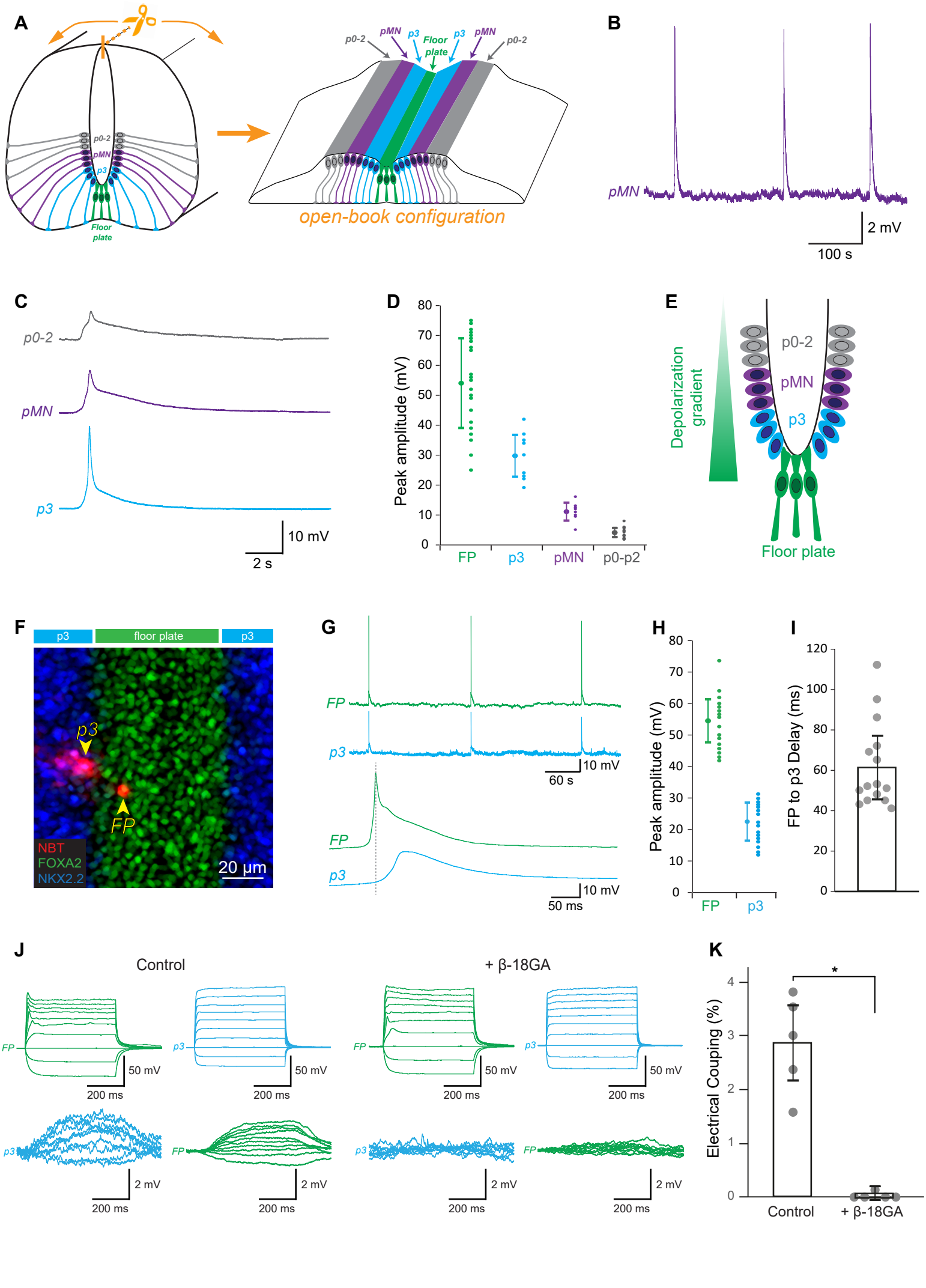
A
p0-2
pMN
p3
Floor plate
open-book configuration
B
pMN
2 mV
100 s
C
p0-2
pMN
p3
10 mV
2 s
D
Peak amplitude (mV)
FP
p3
pMN
p0-p2
E
Depolarization gradient
p0-2
pMN
p3
Floor plate
F
p3
floor plate
p3
NBT
FOXA2
NKX2.2
20 µm
G
FP
p3
10 mV
60 s
50 ms
H
Peak amplitude (mV)
I
FP to p3 Delay (ms)
J
Control
+ β-18GA
50 mV
200 ms
2 mV
K
Electrical Couping (%)
Control
+ β-18GA
*

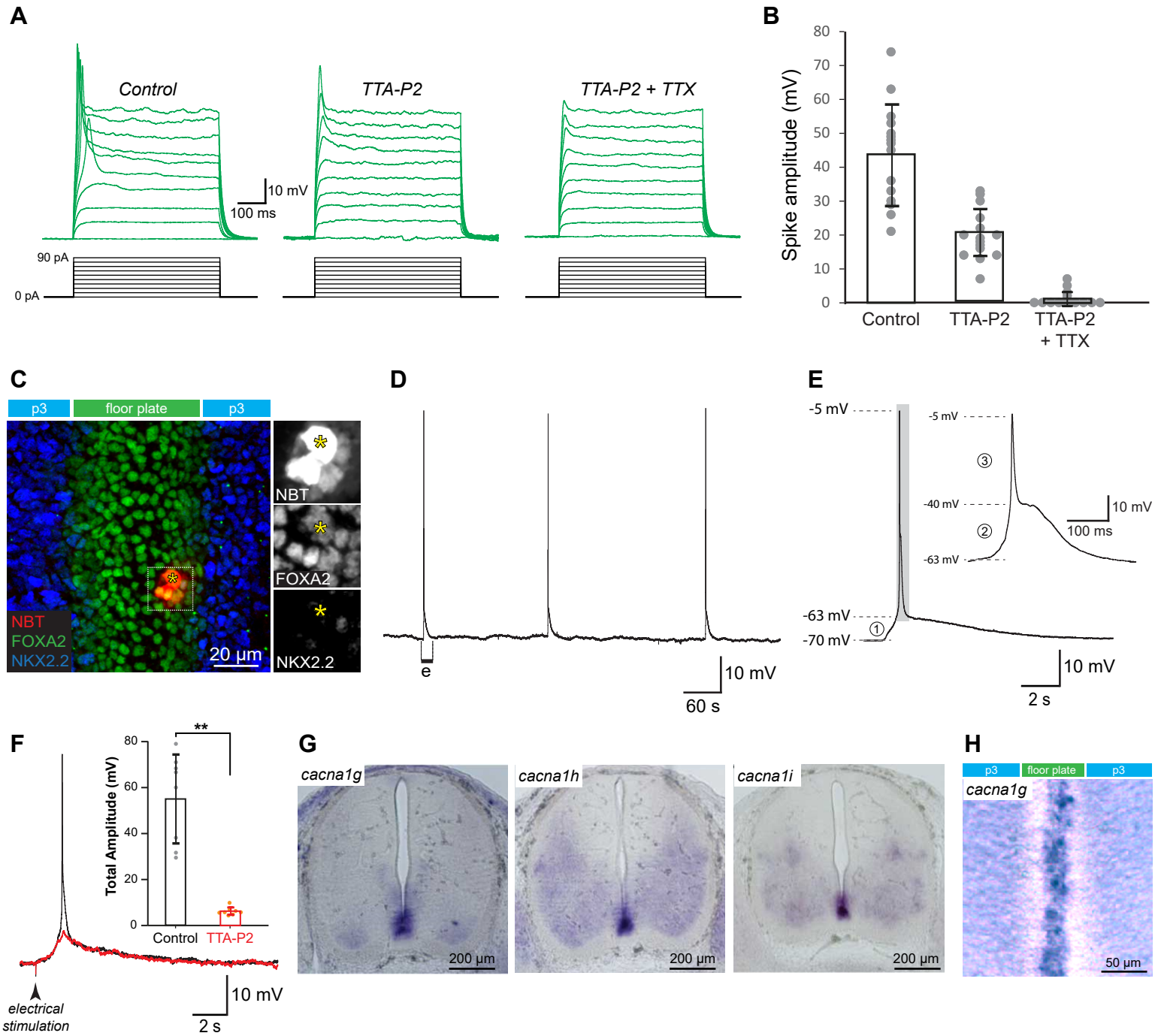
A
Control
TTA-P2
TTA-P2 + TTX
10 mV
100 ms
90 pA
0 pA
B
Spike amplitude (mV)
80
70
60
50
40
30
20
10
0
Control
TTA-P2
TTA-P2
+ TTX
C
p3
floor plate
p3
NBT
FOXA2
NKX2.2
20 µm
NBT
FOXA2
NKX2.2
D
e
10 mV
60 s
E
-5 mV
-40 mV
-63 mV
-70 mV
10 mV
100 ms
10 mV
2 s
F
**
Total Amplitude (mV)
80
60
40
20
0
Control
TTA-P2
electrical
stimulation
10 mV
2 s
G
cacna1g
cacna1h
cacna1i
200 µm
200 µm
200 µm
H
p3
floor plate
p3
cacna1g
50 µm

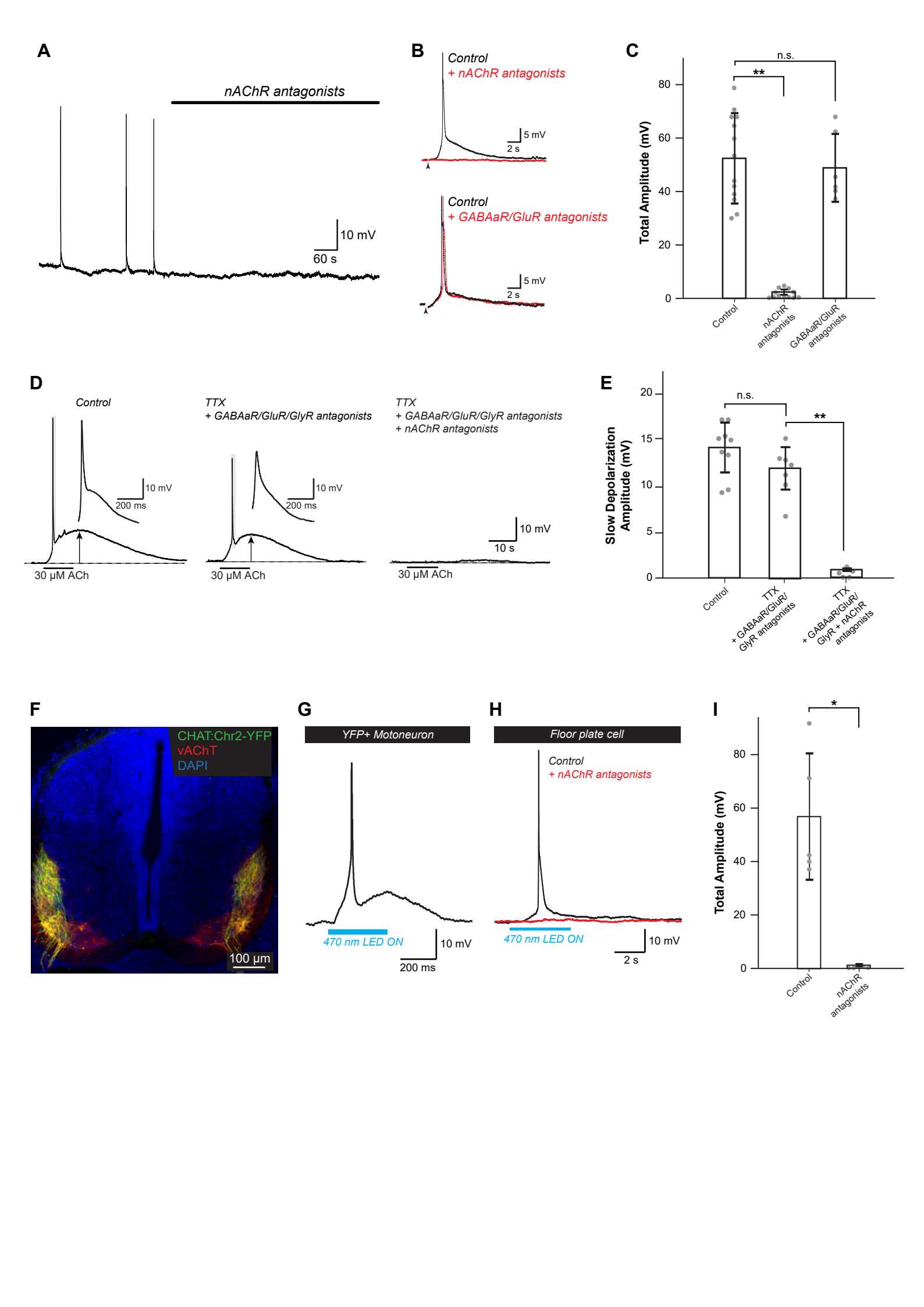
A
nAChR antagonists
10 mV
60 s
B
Control
+ nAChR antagonists
5 mV
2 s
Control
+ GABAaR/GluR antagonists
5 mV
2 s
C
n.s.
**
Total Amplitude (mV)
0
20
40
60
80
Control
nAChR antagonists
GABAaR/GluR antagonists
D
Control
10 mV
200 ms
30 µM ACh
TTX
+ GABAaR/GluR/GlyR antagonists
10 mV
200 ms
30 µM ACh
TTX
+ GABAaR/GluR/GlyR antagonists
+ nAChR antagonists
10 mV
10 s
30 µM ACh
E
n.s.
**
Slow Depolarization Amplitude (mV)
0
5
10
15
20
Control
TTX + GABAaR/GluR/ GlyR antagonists
TTX + GABAaR/GluR/ GlyR + nAChR antagonists
F
CHAT:Chr2-YFP
vAChT
DAPI
100 µm
G
YFP+ Motoneuron
470 nm LED ON
10 mV
200 ms
H
Floor plate cell
Control
+ nAChR antagonists
470 nm LED ON
10 mV
2 s
I
*
Total Amplitude (mV)
0
20
40
60
80
Control
nAChR antagonists

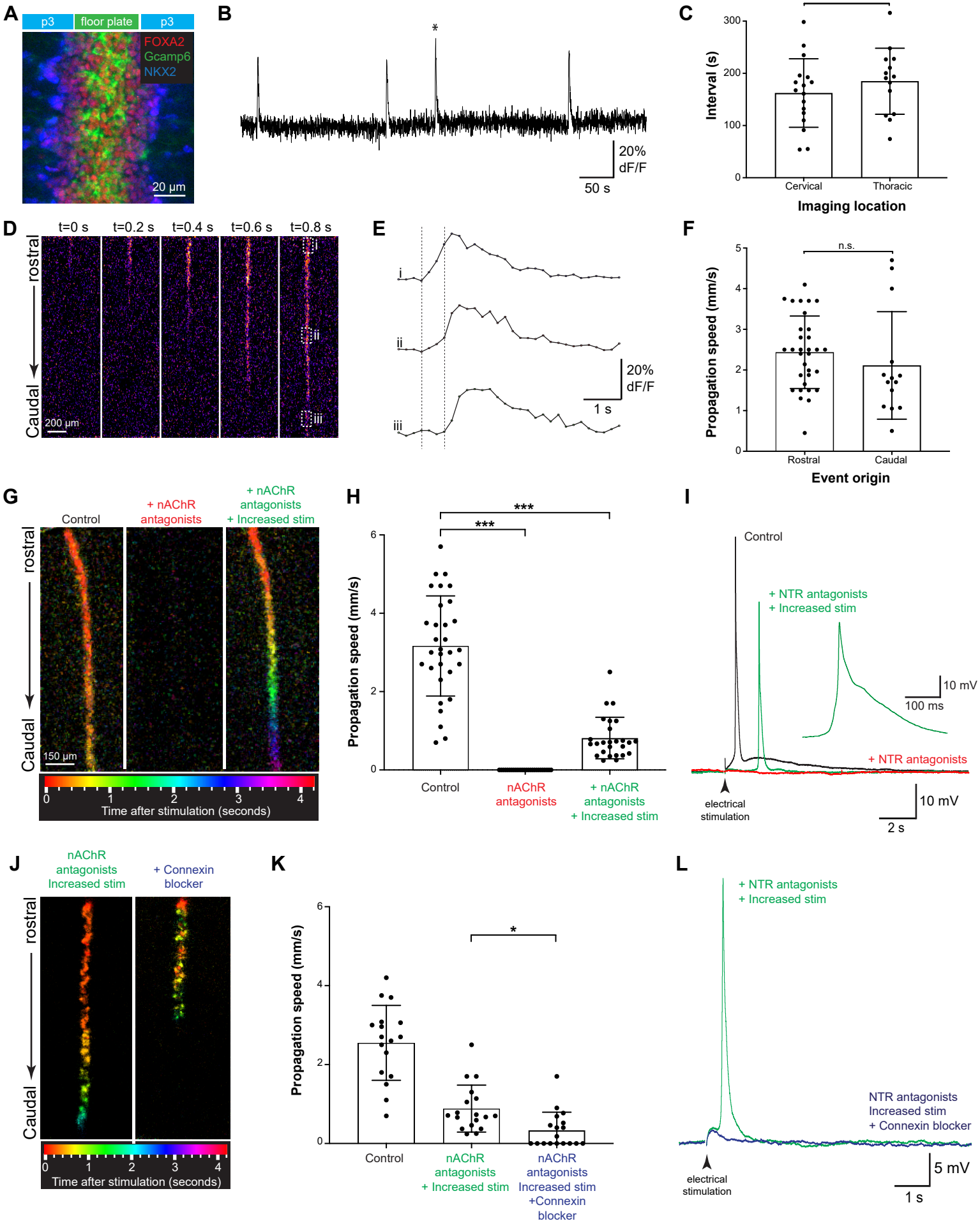
A
p3
floor plate
p3
FOXA2
Gcamp6
NKX2
20 µm
B
*
20%
dF/F
50 s
C
n.s.
Interval (s)
300
200
100
0
Cervical
Thoracic
Imaging location
D
t=0 s
t=0.2 s
t=0.4 s
t=0.6 s
t=0.8 s
rostral
Caudal
200 µm
i
ii
iii
E
i
ii
iii
20%
dF/F
1 s
F
n.s.
Propagation speed (mm/s)
5
4
3
2
1
0
Rostral
Caudal
Event origin
G
Control
+ nAChR antagonists
+ nAChR antagonists + Increased stim
rostral
Caudal
150 µm
0
1
2
3
4
Time after stimulation (seconds)
H
***
***
Propagation speed (mm/s)
6
4
2
0
Control
nAChR antagonists
+ nAChR antagonists + Increased stim
I
Control
+ NTR antagonists + Increased stim
10 mV
100 ms
+ NTR antagonists
electrical stimulation
10 mV
2 s
J
nAChR antagonists Increased stim
+ Connexin blocker
rostral
Caudal
0
1
2
3
4
Time after stimulation (seconds)
K
*
Propagation speed (mm/s)
6
4
2
0
Control
nAChR antagonists + Increased stim
nAChR antagonists Increased stim +Connexin blocker
L
+ NTR antagonists + Increased stim
NTR antagonists Increased stim + Connexin blocker
electrical stimulation
5 mV
1 s

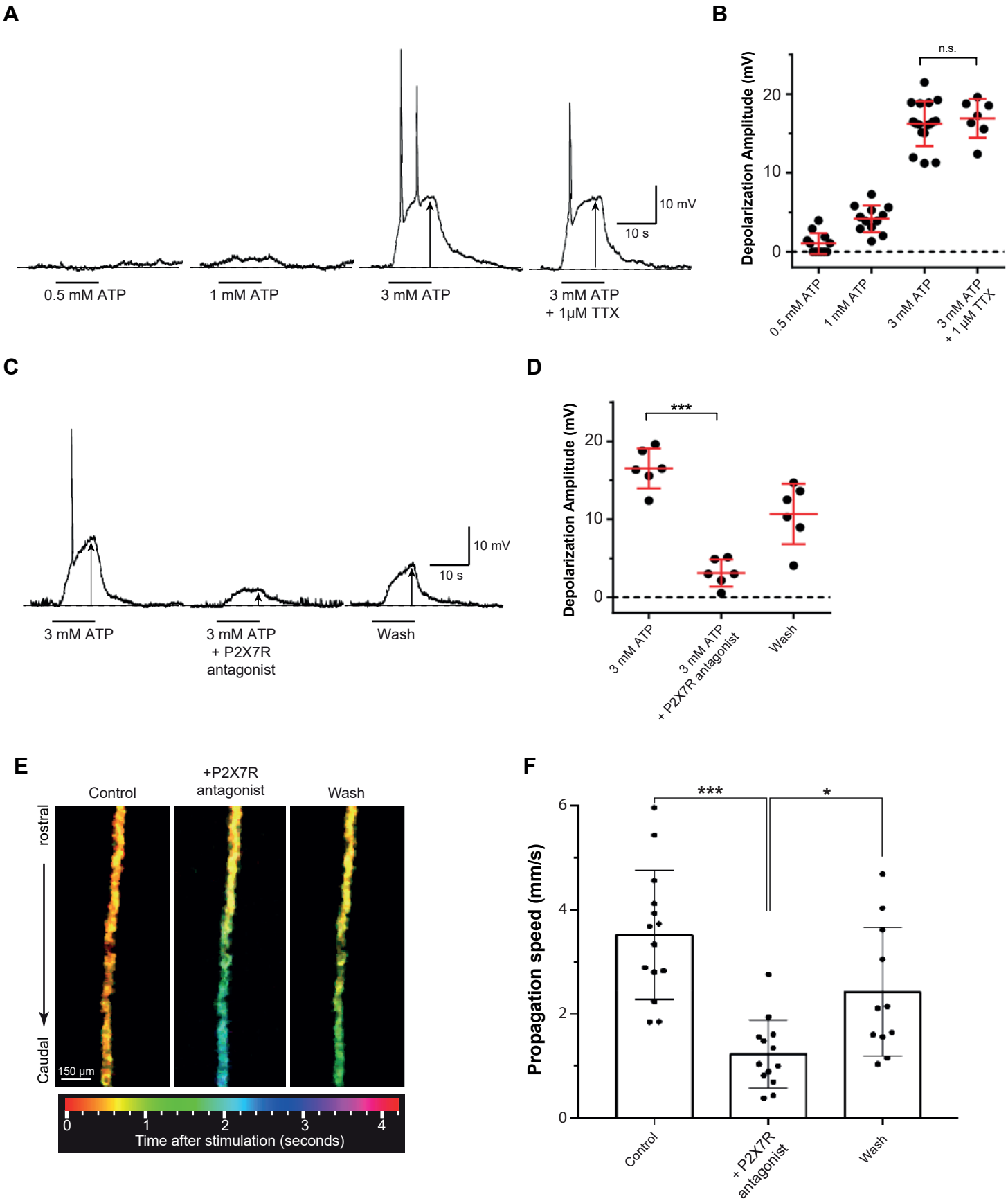
A
10 mV
10 s
0.5 mM ATP
1 mM ATP
3 mM ATP
3 mM ATP
+ 1µM TTX
B
n.s.
Depolarization Amplitude (mV)
20
10
0
0.5 mM ATP
1 mM ATP
3 mM ATP
3 mM ATP
+ 1 µM TTX
C
10 mV
10 s
3 mM ATP
3 mM ATP
+ P2X7R
antagonist
Wash
D
***
Depolarization Amplitude (mV)
20
10
0
3 mM ATP
3 mM ATP
+ P2X7R antagonist
Wash
E
Control
+P2X7R
antagonist
Wash
rostral
Caudal
150 µm
0
1
2
3
4
Time after stimulation (seconds)
F
***
*
Propagation speed (mm/s)
6
4
2
0
Control
+ P2X7R
antagonist
Wash

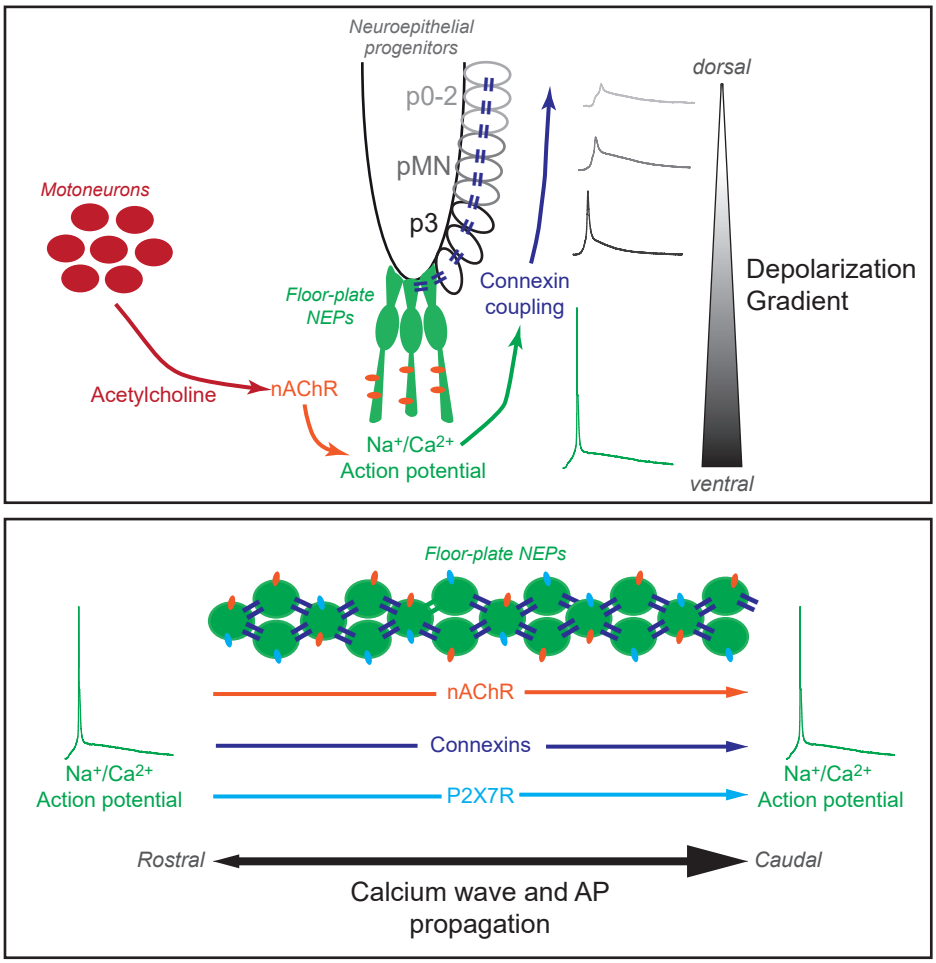
Neuroepithelial progenitors
dorsal
p0-2
pMN
p3
Motoneurons
Floor-plate NEPs
Connexin coupling
Depolarization Gradient
Acetylcholine
nAChR
Na+/Ca2+ Action potential
ventral
Floor-plate NEPs
nAChR
Connexins
P2X7R
Na+/Ca2+ Action potential
Na+/Ca2+ Action potential
Rostral
Caudal
Calcium wave and AP propagation